Polarization-Independent Multi-Resonance With High Q-Factor for Highly Sensitive Terahertz Sensors Based on All-Dielectric Metasurface

Ming Zhang, Ze Ma, Mengxue Yang, Jinyuan Zhao, Baozhu Wang, Weimin Hou, Wanmei Zhang, Cong Li, and Zhonghao Luo

***Abstract*—Since the fingerprints of numerous crucial biologic materials can be identified by terahertz (THz) spectroscopy, THz sensing have become an important approach of biological and medical detections. Particularly, benefit from the excellent capability of metasurface, strong interactions between the metasurface and THz waves can be realized, thus the THz sensing with high sensitivity becomes reality. However, the common configuration of metasurface-based THz sensor is composed of metallic subwavelength structure. Due to the inherent resistive loss of metal, it is still a great challenge to further enhance the quality factor (*Q*-factor) of resonance and sensitivity of THz sensor. In this work, we designed an all-dielectric metasurface with high *Q*-factor for highly sensitive THz sensors. The metasurface is a windmill-like structure consisting of four cuboids, and every adjacent two cuboids are arranged alternately vertically and horizontally. The transmission spectrum of metasurface exhibits four polarization-independent and strong resonance peaks with high *Q*-factor in 0.1–2.5 THz, and all of them show high sensitivity related to ambient refractive index. The transmitted structure and polarization-independent resonances can relief the difficulty of measurement. We believe these studies will lay the theoretical and technical foundation for the design of high-sensitivity terahertz sensing.**

***Index Terms*—Metasurface, terahertz sensor, high quality factor, polarization independence, multiple resonances.**

I. Introduction

TO DATE, electromagnetic waves in the terahertz (THz) frequency range (0.1–10 THz) are used in a wide range of applications, from communications and imaging to gas sensing and pharmaceutical industries, as well as various security and biomedical testing applications, which requires highly sensitive and broadband THz related instruments [1]–[4]. THz waves possess the characteristics of non-ionizing radiation and is very sensitive to weak resonance [5], [6]. However, the relatively large wavelength is longer than the size of the analyte, which leads to insufficient interaction between them [7]–[9]. Then, thanks to the emergency of the metasurface, it is possible to realize high-sensitivity sensor, because the metasurface can induce the intense resonance [10]. Moreover, the resonance is particularly sensitive to the surrounding environment [11]. This unique property enables metasurfaces to provide an excellent platform for biosensing, from microwave to visible frequencies [12]–[14]. Therefore, the research of THz metasurface biosensor has been widely used in biological solution, microbial detection, tumor cell screening and other biomedical directions [15]–[17]. In order to obtain better detection performance, a high-quality factor and ultra-narrow band is particularly crucial for resonance metasurface [18]–[19].

In 2007, Driscoll et al. proposed the first metasurface for THz sensing, designing nanostructure (now widely referred to as metasurfaces) consisting of classical gold-split resonance rings (SRRs) [20]. In 2011, Jansen et al. proposed a horizontally symmetric but vertically asymmetric D-split resonator [21]. Then, Ahmadivand et al designed sensitive metasensors based on plasmonic metasurface by introducing toroidal resonances to achieve the rapid and precise detection of biomarker [22], [23]. In 2021, Recently, M. Askari et al designed a plasmonic metasurface composed of two perpendicularly intersecting metallic bars, whose quality factor and sensitivity can even reach values as high as 3052.75 and 7000 nm/RIU [24]. Among these works, the metal was employed to construct the plasmonic metasurface to achieve metasensor for detecting biomolecules. However, the metallic materials used in the metasurfaces inevitably produces ohmic and radiation losses [25], limiting further improvements in sensitivity. As one of the excellent alternatives of plasmonic metasurface, all-dielectric metasurface can support Mie resonance (electric dipole, magnetic dipole, and other multipole resonances) with low dissipation and low thermal conductivity [26]–[28]. In 2019, He et al. proposed the Si-ADMS structure, utilizing the asymmetry of the structure to achieve a quality factor exceeding 60 [29]. In 2021, Li et al. proposed an all-dielectric columnar structure with asymmetry [30], which also achieved Fano resonance with a very high *Q*-factor. Although

Manuscript received 1 July 2022; revised 26 July 2022; accepted 30 July 2022. Date of publication 3 August 2022; date of current version 15 August 2022. This work was supported in part by the National Natural Science Foundation of China under Grant 62105093, in part by the Doctoral Research Initializing Fund of Hebei University of Science and Technology under Grant 1181382, in part by the College Students' Innovation and Entrepreneurship Training Program of Hebei province under Grant S202110082033, and in part by the Special project of cultivating scientific and technological innovation ability of college students in Hebei Province under Grant 22E50066D. *(Corresponding authors: Ming Zhang; Weimin Hou.)*

The authors are with the School of Information and Engineering, Hebei University of Science and Technology, Shijiazhuang 050018, China (e-mail: zhangming5280@126.com; 1938627202@qq.com; 2836804469@qq.com; zhaojinyuanyy@yeah.net; wangbz@hebust.edu.cn; hwm@hebust.edu.cn; 805735443@qq.com; 656677599@qq.com; 1184950638@qq.com).

Digital Object Identifier 10.1109/JPHOT.2022.3196022

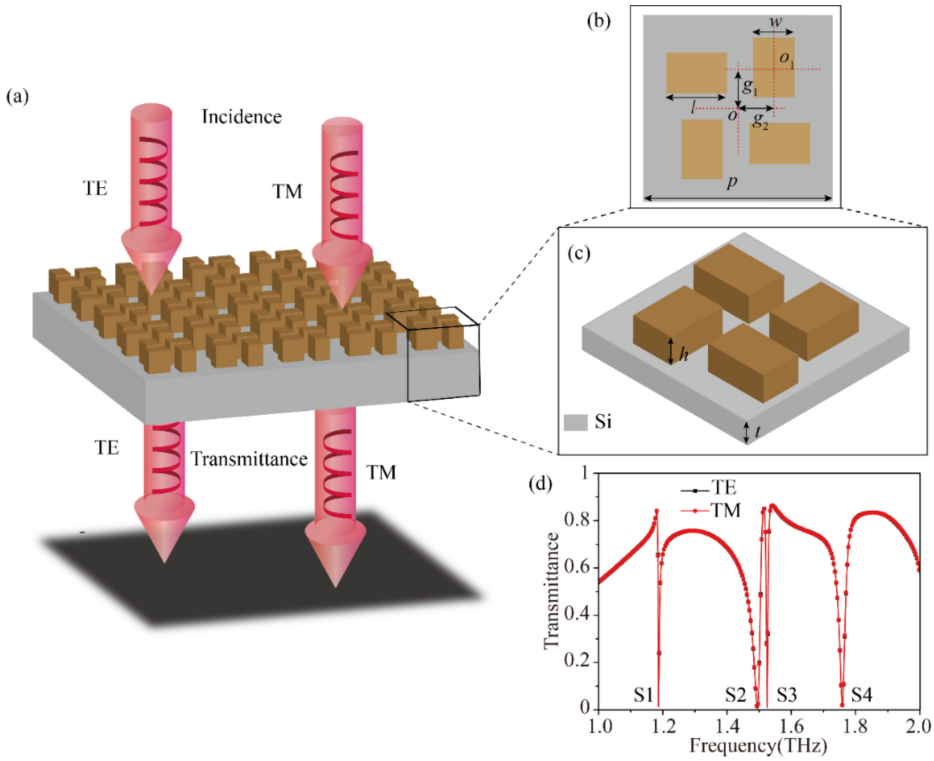

Fig. 1. Schematic diagram of THz metasurface and its simulated results. (a) The schematic diagram of the metasurface under the incidence of TE and TM mode, and the metasurface is a transmitted structure. (b) Top view of the metasurface with geometric parameters. (c) Three-dimensional illustration. (d) Simulated transmission spectra at normal incidence under TE and TM modes.

all-dielectric materials avoid the loss caused by metal materials, asymmetric structure will cause polarization dependence (i.e., inconsistent spectral results in TE and TM directions) which hinders the further improvement of sensitivity and increases the difficulty of measurement. Moreover, most of the previous metasurfaces can only generate one single resonance, leading weak detection capability.

In this work, we designed an all-dielectric metasurface with high *Q*-factor for highly sensitive THz sensors. The metasurface is designed by the principle of locally asymmetry but entirely symmetry, and the metasurface is a windmill-like structure consisting of four cuboids. The entirely symmetry structure ensures the polarization independence in spectral responses. Every adjacent two cuboids are arranged alternately vertically and horizontally, and the unequal length and width introduces the local asymmetry, which can excite the high-quality resonances. The transmission spectra of metasurface exhibit four polarization-independent and strong resonance peaks with high *Q*-factor in 0.1-2.5 THz, and the *Q*-factors are 320, 93.4, 412, and 117, respectively. These resonance peaks show high sensitivity related to ambient refractive index, where the frequency sensitivities of S2 (1.4946 THz) and S4 (1.7587 THz) are 273 and 105 GHz/RIU, respectively. Besides, the corresponding sensitivity of these resonance can still reach 344.4GHz/RIU and 571.36% RIU^{-1} (defined by amplitude change) when capped on a lossy analyte. The transmitted structure and polarization-independent resonances can relief the difficulty of measurement. We believe these studies will lay the theoretical and technical foundation for the design of high-sensitivity THz sensing.

II. Design and Simulations

We designed a transmitted and all-dielectric metasurface based on the design principle of locally asymmetry but entirely symmetry, which is illustrated in the Fig. 1(a). The overall structure is symmetry, and thus, the spectral responses to TE and TM polarized incidence are consistent. In addition, the designed metasurface is transmitted structure, so we can easily measure its transmission in practical. The top view of the metasurface is shown in Fig. 1(b). The metasurface is a centrosymmetric structure consisting of four identical cuboids, which can be regarded as a cuboid rotated four times clockwise or counterclockwise around an axis parallel to the *z*-direction passing through the center of unit cell. The length and width of cuboids are represented by l and w. The distance between the center of each cuboid in the direction of the long edge and the line passing through the center point o (the line is perpendicular to the long edge of the cuboid) is g_1. The distance between the center of each cuboid in the direction of the short edge and the line passing through the center point o (the line is perpendicular to the short edge of the cuboid) is g_2. The metasurface is arranged periodically with a period p. The three-dimensional view of the metasurface is shown in Fig. 1(c). The upper layer is gallium arsenide (GaAs), and the thickness is denoted by h. The substrate is intrinsic silicon (Si), and the thickness is denoted by t.

We used a commercial software package CST Microwave Studio 2018 to model and analyze the metasurface with finite element method. The relative permittivity of silicon is 11.9, and its electric conductivity is 2.5×10^4 S/m [31]. Under equilibrium condition, the complex dielectric function of GaAs, $\varepsilon_{\text{GaAs}}$ can be expressed by the Drude model as [32]:

$$\varepsilon_{\text{GaAs}} = \varepsilon_\infty - \frac{\omega_p^2}{\omega^2 + i\omega\gamma} \tag{1}$$

Where, ε_∞ is 12.94 when frequency is infinite. The plasma frequency of GaAs is 6.16×10^8 Hz. The boundary conditions in the *x* and *y* directions are set as unit cell, while the open boundary condition is applied to the *z* direction. The background distances along *z* direction (both the upper and lower *z* distance) are set as 1000 μm. To demonstrate the polarization independence of the THz metasurface, the normally incident TE- and TM-polarized plane waves are both applied in the simulations. The optimized geometric parameters are as follows: $p = 100$ μm, $l = 42$, $w = 22$ μm, $g_1 = 22$ μm, $g_2 = 19$ μm, $h = 30$ μm, and $t = 25$ μm. Since the common thickness of silicon wafer is approximately 500-600 μm, we can use the silicon backside thinning technology involving wet etching and chemical mechanical polishing to realize such optimal thickness of the silicon substrate in the simulation.

The transmission spectra of proposed metasurface under TE- and TM-polarized waves are depicted in Fig. 1(d). To begin with, the simulated transmission spectra in the TE mode (the black line with rectangle symbol) and TM mode (the red line with circle symbol) are consistent in the frequency range of 1-2 THz, indicating the polarization independency of the designed metasurface. As shown in the figure, four resonance peaks with high *Q*-factor are located at 1.1868 THz, 1.4946 THz, 1.5250 THz and 1.7587 THz, respectively. For simplicity of description, these four resonances are denoted by S1, S2, S3, and S4. The corresponding *Q*-factor is attained from $Q = f_0$/FWMH, where f_0 denotes the resonance frequency and FWHM represents the full width at half maximum of transmission spectrum [31]. Accordingly, the calculated *Q*-factors of four resonances are 320, 93.4, 412, and 117, respectively. Because THz metasurfaces are sensitive to the surrounding analyte, so they can act as THz sensor by measuring their frequency shift or amplitude change. In the field of sensing, the high *Q*-factor resonances with extremely narrow resonant bandwidth is one of the most crucial elements for highly sensitive sensors. Therefore, the high *Q*-factors of the four resonances imply that the metasurface can be functioned as a highly sensitive sensor in THz range. Moreover, these multiple resonances can complement each other during measurement, realizing the sensing detection of various materials. The transmitted metasurface with polarization independency and multiple high *Q*-quality resonances is designed based on the principle of locally asymmetry but globally symmetry. Since the THz metasurface possesses the large period (generally tens to hundreds of microns), so the metasurface can be designed with complex structure based on the large degrees of design freedom. Relying on the advantage, four identical cuboids are designed to be centrosymmetric, but in which each group of two adjacent cuboid is asymmetric for introducing the high *Q*-quality resonance [33]. The entire structure is centrosymmetric, accordingly, to avoid the asymmetric structure caused by the inconsistent results TE and TM mode [34]. By using this method, polarization insensitive and multi-resonant metasurface can be obtained, which is beneficial to improve the sensitivity of sensors.

III. Results and Discussions

To explain the physical mechanism of these four resonances, the instantaneous electric and magnetic field distributions of the metasurface in the *x*-*y* plane at resonant frequencies (1.1868 THz, 1.4946 THz, 1.5250 THz and 1.7587 THz) under TE mode are depicted in Fig. 2. Due to the polarization independency of the spectral responses, we only illustrated the distribution of electric field and magnetic field in TE mode. Fig. 2(a) shows that at 1.1868 THz, the strong electric field is distributed in the four corners of the cuboid in the lower left corner and the upper right corner. Between the adjacent corners of these two cuboids, the mutual influence of the electric field makes the electric field intensity maximum. As shown in Fig. 2(b), the magnetic field is confined inside the cuboids at the resonance frequency of 1.4946 THz. The charge distributions at the upper and lower sides of parallel cuboids are opposite, which indicates that the current induced by resonance flow along the two cuboids based on Ampère's law, as depicted in Fig. 2(c). Since the directions of the induced current can be found from the directions of Ez near the elliptical cylinders, induced currents in the cuboids are in anti-phase at the Fano resonance mode as shown by red arrows. These anti-phase oscillations result in decrease of the loss at resonance, leading a high *Q*-factor. As shown in Fig. 2(d), the magnetic field distribution constitutes the magnetic quadrupole mode, which is marked in red dotted circle. At frequency of 1.5250 THz, the electric field at this frequency is concentrated in the center of symmetry and close to the upper left and lower right cuboids, which is shown in Fig. 2(e). In addition, there are strong electric fields on the edge sides of the lower left and upper right cuboids of the unit cell. Therefore, the magnetic field at this resonance frequency are confined in the center of these four cuboids, as depicted in Fig. 2(f). The electric field distribution at the frequency of 1.7587 THz is shown in Fig. 2(g). We find that there are strong electric fields around the cuboid at the upper right and lower left in each unit cell, which indicates that the current flow along the upper adjacent two cuboids is opposite to that along the lower adjacent two cuboids. The electric field distributions at this resonance frequency form the electric quadrupole mode, which is marked by red dotted circle. The anti-phase current induces a magnetic quadrupole mode in the cuboids, as shown in Fig. 2(h). Similarly, the anti-phase oscillations result in decrease of radiative loss at resonance, exhibiting a high *Q*-factor. The coupling between these four cuboids introduces multiple resonance, and the symmetry of entire metasurface makes it polarization independent. These characteristics have provided the possibility of designed metasurface to be regarded as highly sensitive THz sensor.

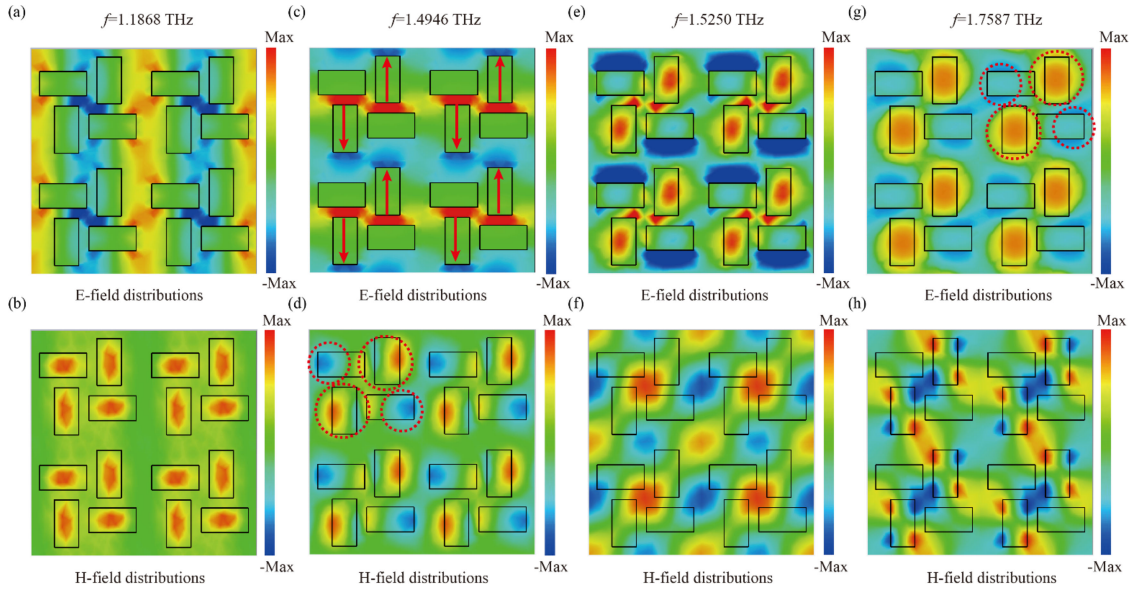

Fig. 2. The electric and magnetic field distribution in the x-y plane at four resonance frequencies. Electric field distribution at frequency of 1.1868 THz (a), 1.4946 THz (c), 1.5250 THz (e), and 1.7587 THz (g). Magnetic field distribution at frequency of 1.1868 THz (b), 1.4946 THz (d), 1.5250 THz (f), and 1.7587 THz (h).

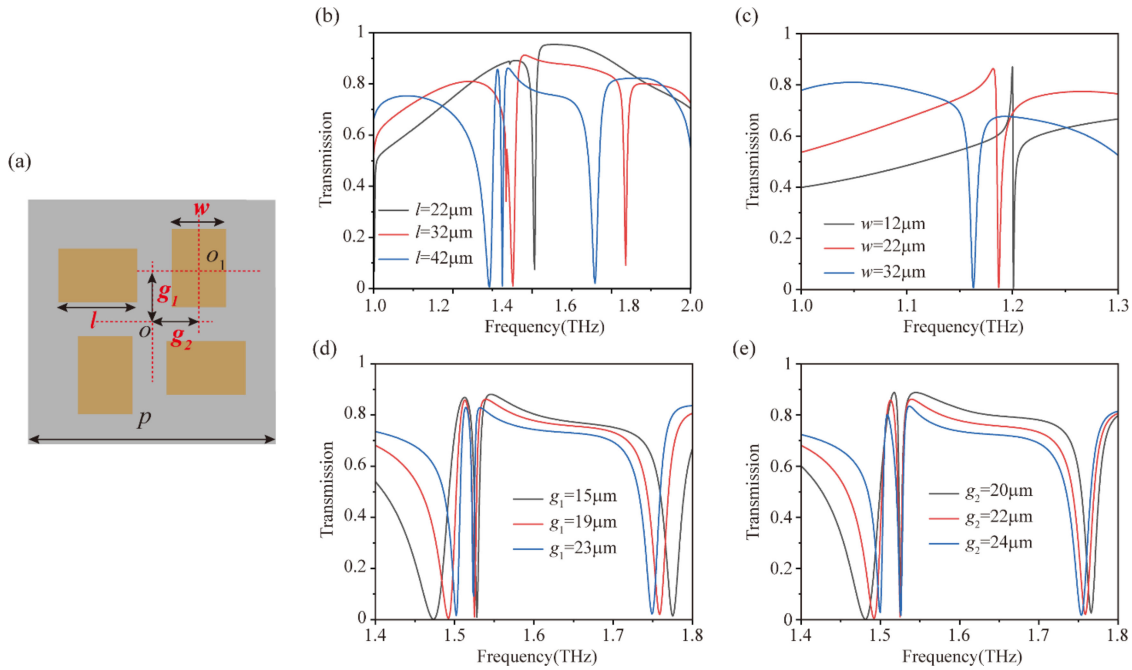

Fig. 3. The simulated transmission spectra of metasurface with geometric parameter sweep. (a) the top view of metasurface with geometric parameters, the scanning parameters were highlighted in red. (b) the transmission spectra with different lengths l of bars. (c) the transmission spectra with different width w of bars. (d) the transmission spectra with different gaps g_1. (e) the transmission spectra with different gaps g_2.

By changing the geometric parameters, we analyze the effects of different parameters on the spectral responses and better interpret the inner physical mechanism. Fig. 3(a) shows the top view of the metasurface with geometric parameters, where the analyzed geometric parameters are highlighted in red. To clearly describe the influence of geometric parameters on spectral responses of the designed metasurface, we only show resonances that are greatly affected when geometric parameters change. Fig. 3(b) shows the simulation results of the change of length l, while the other geometric parameters are fixed to optimal values. It can be seen from the figure that as the value of l increases, all resonance peaks redshift and even resonance S1 cannot be observed in the range of 1–2 THz. Moreover, when $l = 22$ μm (representing that $l = w$ and the local asymmetry disappears),

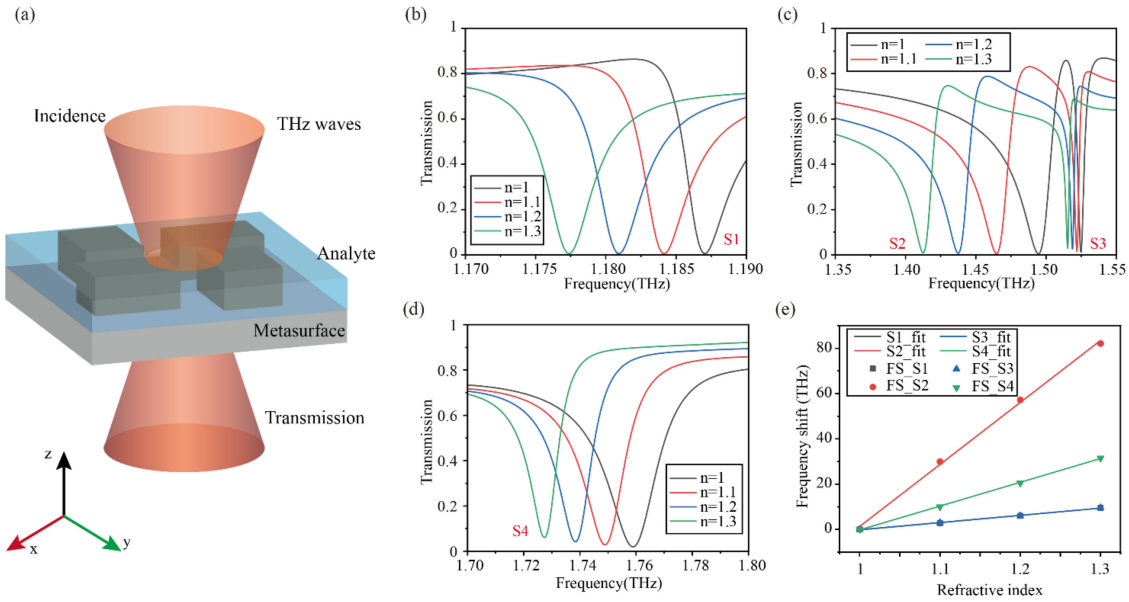

Fig. 4. The simulated sensing characteristic of the designed metasurface. (a) Schematic of the all-dielectric metasurface sensor with under-test analyte. Transmission spectra of varied refractive index from 1.0 to 1.8 with analyte thickness of 30 μm. (a), (b) and (c) Illustrate the corresponding electromagnetic response of S1 to S4, respectively. (d) The frequency shifts and their fitting curve of the resonance S1 to S4.

resonance S2 and S4 disappear, which is depicted in black line. The simulation results indicate that the resonances S2 and S4 are induced by local asymmetry of metasurface. As the increase of *l*, the asymmetry is introduced in metasurface, thus the resonances S2 and S4 appear in this frequency range. Besides, the bandwidth of resonance peaks becomes wider, that is, the *Q*-factors of resonances are decrease. Since the electromagnetic waves are confined in the structure at quadrupole mode, an anti-parallel current is generated in the parallel cuboids. The increase of *l* results in the cuboids becoming larger, so the *Q*-factors decreases. Fig. 3(c) shows the simulation results of the scanning width *w*. Apparently, with the increase of *w,* the resonance S2 redshifts, and its bandwidth becomes wider. This is because the increase of *w* leads to the gradual approach of the width and length of the cuboid and the reduction in asymmetry degree, so the Fano resonance becomes weaker and the *Q*-factor of S2 increases. Fig. 3(d) and (e) show the simulation results of the change of g_1 and g_2, and these two parameters have same influence on the resonance S2 and S4. With the increase of g_1 and g_2, the resonances S2 and S4 redshift, and the bandwidth of S2 becomes wider. The difference is that the effect of g_1 on the electromagnetic response is greater. The reason why bandwidth of S2 becomes wider with the increase of g_1 and g_2 is that the increasing gap enlarges the distance between the adjacent cuboids, reducing the confinement of electric field by Fano resonance. However, the influence of variable gap on the resonances S1 and S2 is slight. Because the resonances occur insides the cuboids, and thus the increase of gap indeed affects the resonances. The simulation results of geometric parameters scanning analysis can further interpret the physical mechanism of the multiple high *Q*-factor resonances. Besides, the influence of geometric parameters on electromagnetic responses is helpful for metasurface design in another working frequency range.

VI. Characteristics of Sensing

Regarding some metasurfaces, when illuminated by EM waves on the under-test sample (an analyte capped on the metasurface), the resonance frequency shift or amplitude change occurs in the spectral response with respect to the empty structure. This is the key to realize the refractive index sensing of metasurfaces. We simulated the characteristic of sensing by covering the analytes with different refractive indexes (thickness of 30 μm) capped on the metasurface. Fig. 4(a) shows the schematic diagram of the metasurface as THz sensor covered with under-test analyte. The simulation results of frequency shift are shown in Fig. 4(b), (c) and (d). When the refractive index n increases from 1.0 to 1.3 with the increment of 0.1, all the resonances exhibit obvious red shift of frequency. To characterize the performance of the designed metasurface, the frequency sensitivity (FS) can be calculated by

$$FS = \frac{\Delta f(\mathrm{GHz})}{\Delta n(\mathrm{RIU})} \tag{2}$$

Where $\Delta \mathrm{n} = \mathrm{n_a} - \mathrm{n_0}$ with $\mathrm{n_a}$ is the refractive index of analyte and $\mathrm{n_0}$= 1 represents without analyte. $\Delta f = f_a - f_0$ with f_a is the resonance frequency when the refractive index of the analyte is $\mathrm{n_a}$, and f_0 is the resonance frequency of empty metasurface. According to the equation, we can calculate that the FS of S1 to S4 are 32, 273, 31.8 and 105 GHz/RIU, respectively. To accurately describe the sensitivity of the metasurface, we extracted the sampling points of the frequency shift and conducted curve fitting, which is depicted in Fig. 4(e). Obviously, there is a

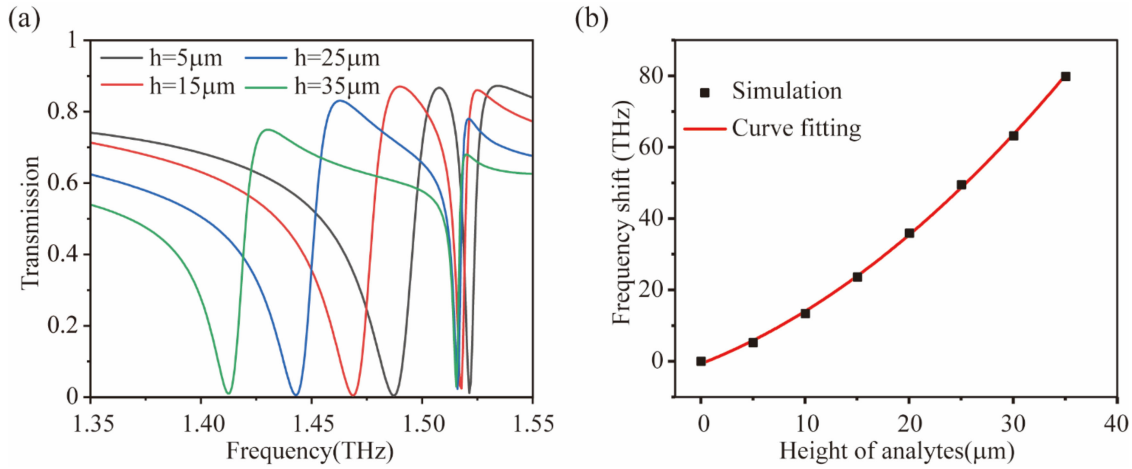

Fig. 5. (a) Transmission spectra of varied analyte thickness from 5 to 35 μm with the fixed refractive index n = 1.3. (b) The extracted sampling points of the frequency shift and its fitting curve in varied analyte thickness.

TABLE I
THE EQUATION AND FITTING DEGREE OF THE FITTING CURVE

Resonance	Equation of fitting curve	Fitting degree (R^2)
S1	y1=32x-32.2	0.9969
S2	y2=273.6x-272.3	0.9983
S3	y3=31.8x-31.92	0.9968
S4	y4=105x-105.2	0.9995

linear relationship between frequency shift and refractive index change. These linear relationship of S1 to S4 are illustrated in the Table I. The simulated results indicates that these four resonances possess good sensing performance. Furthermore, the figure of merit (FoM) is also considered to identify the actual performance of the sensor defined as FoM = FS/FWHW, where FS is the frequency sensitivity and FWHM is the full width at half maximum [24]. For the resonance S2 and S4, the FS are 273 and 105 GHz/RIU, and the FWHM are 1.6 and 1.5 GHz. Therefore, the FoM of S2 and S4 are calculated as 170.6 and 70, respectively. The calculated results indicate that the proposed metasurface has significant performance in THz sensing.

Moreover, the thickness of analyte plays an important role in the resonance frequency shift, which is also investigated in the simulations. The refractive index of different thickness is fixed as n = 1.3. As shown in Fig. 5(a), with the analyte thickness increases, the resonance frequency of S2 shifts red with the total frequency shift of 80.1GHz when the thickness changes from 5 to 35 μm. The resonance frequency redshift is generally attributed to the enhanced net capacitive of the structure that results from the increased analyte thickness. Specifically, the fringing fields at capacitive gaps, where the analyte is placed, are mainly responsible for causing the redshift. In the same way, the FS of analyte thickness can also be defined using (2), just replace Δn with Δd. d is the thickness of analyte. Fig. 5(b) shows the extracted sampling points of the frequency shift and its fitting curve. The relationship between the analyte thickness and frequency shift can be described as y = 0.03352x^2+1.134x-0.6917 with the fitting degree of R^2 = 0.9996. The simulation results imply that the designed all-dielectric metasurface has feasible capability for biological and chemical sensing in THz range.

Under the condition of only considering the refractive index, we consider the difference between the actual analyte (liquid sample) and the simulated analyte. The actual analyte generally can absorb terahertz waves, which reduces the amplitude of resonance peak. We covered the metasurface sensor with a layer of analyte with the constant tangent loss of 0.1, whose simulated results are shown in Fig. 6(a). Under this condition, we can still clearly observe the resonance peak in the transmission spectrum. Moreover, the frequency shift and amplitude change of the S2 and S4 are still obvious. Similarly, we extract the resonances S2 and S4 to analyze the frequency shift and amplitude change, respectively. The fitting curves are shown in Fig. 6(b). The two straight lines still show a monotonous relationship. The corresponding function of the blue line representing the frequency shift of S2 is y = 344.4x-342.6, so the characteristic peak still has a sensitivity of 344.4GHz/RIU. Considering the sensitivity of S4, we can use the transmission amplitude change to characterize. Replace Δf with Δr in the (2), where $\Delta r = \frac{r_a}{r_0} \times 100\%$ with the resonance amplitude r_a (i.e., the transmittance of resonance S4) when the refractive index of the analyte is n_a. r_0 is the resonance amplitude without analyte. For the resonance S4, the r_0 equals to 0.121 when the refractive index n = 1.0. r_a are 0.185, 0.255, 0.325 when n_a are 1.1, 1.2, and 1.3, respectively. Therefore, the calculated Δr equals to 57.1%, and the and the amplitude sensitivity can be calculated by

$$AS = \frac{\Delta r}{\Delta n} \tag{3}$$

Therefore, the corresponding function of the red line represents the amplitude change of S4 is y = 571x-572.59, so the sensitivity is 571% RIU^{-1}. The metasurface still maintain high

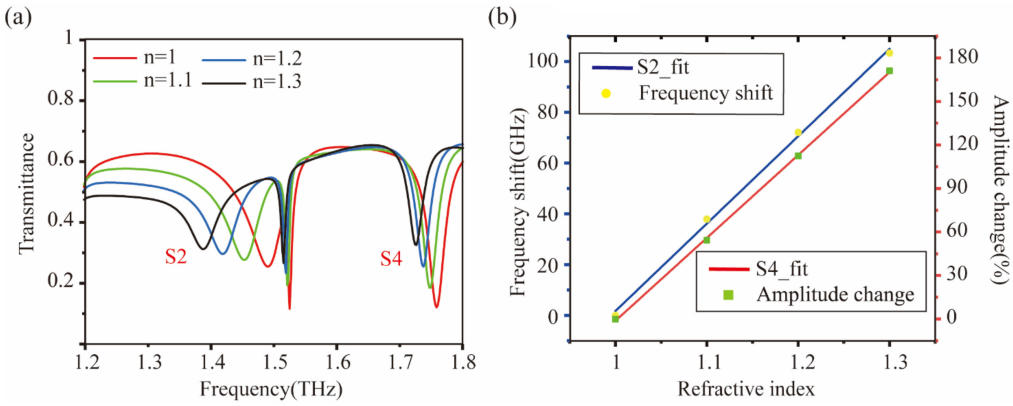

Fig. 6. Results produced by covering the metasurface with lossy analytes. (a) The simulated transmission of metasurface capped on the lossy analyte with different refractive index. (b) Fitted curves of the corresponding frequency shifts and amplitude changes of the resonance at 1.4946 THz and 1.7587 THz.

sensitivity under lossy analyte. Based on the above sensitivity analysis, multiple resonances can provide complementary and mutually verifiable detection for various analytes.

IV. Conclusion

To sum up, we proposed an all-dielectric metasurface to generate polarization-independent and multiple high *Q*-factor resonances. The main part of the metasurface is a windmill-like structure composed of four identical cuboids. Every two adjacent cuboids form an asymmetric structure to induce Fano resonance. The entire centrosymmetric structure ensures that the metasurface is polarization independent. The metasurface possesses four polarization-independent resonances with high *Q*-factor, where the frequency sensitivities of S2 (1.4946 THz) and S4 (1.7587 THz) are 273 and 105 GHz/RIU, respectively. Besides, the corresponding sensitivity of these resonances can still reach 344.4GHz/RIU and 571% RIU^{-1} (defined by amplitude change) when capped on the lossy sample. Moreover, the transmitted structure and polarization-independent resonance can relief the difficulty of measurement. The all-dielectric configuration of metasurface that is designed by the principle of locally asymmetry but globally symmetry can be applied at microwave or infrared band. We believed that this research could promote the development of THz metasurface in biosensing and medical detection.

References

[1] Y. Cheng, H. Zhao, and C. Li, "Broadband tunable terahertz metasurface absorber based on complementary-wheel-shaped graphene," *Opt. Mater.,* vol. 109, no. 1, 2020, Art. no. 110369.

[2] A. E. Yachmenev, D. V. Lavrukhin, I. A. Glinski Y, N. V. Zenchenko, and D. S. Ponomarev, "Metallic and dielectric metasurfaces in photoconductive terahertz devices: A review," *Opt. Eng.,* vol. 59, no. 6, 2019, Art. no. 061608.

[3] X. Du et al., "Highly sensitive detection of plant growth regulators by using terahertz time-domain spectroscopy combined with metamaterials," *Opt. Exp.,* vol. 29, no. 22, pp. 36535–36545, 2021.

[4] T. Cao et al., "Multi-cycle reconfigurable THz extraordinary optical transmission using chalcogenide metamaterials," *Opto-Electron. Sci.,* vol. 1, no. 1, pp. 210010–200011, 2022.

[5] H. Yoshida et al., "Terahertz sensing method for protein detection using a thin metallic mesh," *Appl. Phys. Lett.,* vol. 91, no. 25, 2007, Art. no. 253901.

[6] B. Ferguson and X.-C. Zhang, "Materials for terahertz science and technology," *Nature Mater.,* vol. 1, no. 1, pp. 26–33, 2002.

[7] M. Zhang et al., "Highly sensitive terahertz sensors based on polarization independent and multiple resonance," *Opt. Commun.,* vol. 507, 2022, Art. no. 127519.

[8] M. Beruete and I. Jáuregui-López, "Terahertz sensing based on metasurfaces," *Adv. Opt. Mater.,* vol. 8, no. 3, 2019, Art. no. 1900721.

[9] C. Debus and P. H. Bolivar, "Frequency selective surfaces for high sensitivity terahertz sensing," *Appl. Phys. Lett.,* vol. 91, no. 18, 2007, Art. no. 184102.

[10] A. Nemati, Q. Wang, N. Ang, W. Wang, M. Hong, and J. Teng, "Ultra-high extinction-ratio light modulation by electrically tunable metasurface using dual epsilon-near-zero resonances," *Opto-Electron. Adv.,* vol. 4, no. 7, 2021, Art. no. 200088.

[11] Y. Zhu, A. I. Kuznetsov, B. Luk'yanchuk, N. Engheta, and P. Genevet, "Traditional and emerging materials for optical metasurfaces," *Nanophotonics,* vol. 6, no. 2, pp. 452–471, 2017.

[12] S. Tan, F. Yan, W. Wang, H. Zhou, and Y. Hou, "Ultrasensitive sensing with three-dimensional terahertz metamaterial absorber," *J. Opt.,* vol. 20, no. 5, 2018, Art. no. 055101.

[13] Y. Wang, Z. Han, Y. Du, and J. Qin, "Ultrasensitive terahertz sensing with high-Q toroidal dipole resonance governed by bound states in the continuum in all-dielectric metasurface," *Nanophotonics,* vol. 10, no. 2, pp. 1295–1307, 2021.

[14] M. Zhang et al., "Automatic and inverse design of broadband terahertz absorber based on optimization of genetic algorithm for dual metasurfaces," *Opt. Exp.*, vol. 30, pp. 22974–22985, 2022.

[15] C. Yu, S. Fan, Y. Sun, and E. Pickwell-Macpherson, "The potential of terahertz imaging for cancer diagnosis: A review of investigations to date," *Quantum Imag. Med. Surg.,* vol. 2, no. 1, pp. 33–45, 2012.

[16] M. Tonouchi, "Cutting-edge terahertz technology," *Nature Photon.,* vol. 1, pp. 97–105, 2007.

[17] A. Ahmadivand and B. Gerislioglu, "Photonic and plasmonic metasensors," *Laser Photon. Rev.*, vol. 16, no. 2, 2022, Art. no. 2100328.

[18] X. Long, M. Zhang, Z. Xie, M. Tang, and L. Li, "Sharp Fano resonance induced by all-dielectric asymmetric metasurface," *Opt. Commun.,* vol. 459, no. 1, 2020, Art. no. 124942.

[19] R. Singh, W. Cao, I. Al-Naib, L. Cong, W. Withayachumnankul, and W. Zhang, "Ultrasensitive terahertz sensing with high-Q Fano resonances in metasurfaces," *Appl. Phys. Lett.,* vol. 105, no. 17, 2014, Art. no. 171101.

[20] T. Driscoll, G. O. Andreev, D. N. Basov, S. Palit, and D. R. Smith, "Tuned permeability in terahertz split-ring resonators for devices and sensors," *Appl. Phys. Lett.,* vol. 91, no. 6, 2007, Art. no. 062511.

[21] C. Jansen, I. Al-Naib, N. Born, and M. Koch, "Terahertz metasurfaces with high Q-factors," *Appl. Phys. Lett.,* vol. 98, no. 5, 2011, Art. no. 051109.

[22] A. Ahmadivand et al., "Rapid detection of infectious envelope proteins by magnetoplasmonic toroidal metasensors," *ACS Sensors*, vol. 2, no. 9, pp. 1359–1368, 2017.

[23] A. Ahmadivand et al., "Extreme sensitive metasensor for targeted biomarkers identification using colloidal nanoparticles-integrated plasmonic unit cells," *Biomed. Opt. Exp.*, vol. 9, no. 2, pp. 373–386, 2018.

[24] M. Askari, H. Pakarzadeh, and F. Shokrgozar, "High Q-factor terahertz metamaterial for superior refractive index sensing," *J. Opt. Soc. Amer. B*, vol. 38, pp. 3929–3936, 2021.

[25] X. Liu, K. Fan, I. V. Shadrivov, and W. J. Padilla, "Experimental realization of a terahertz all-dielectric metasurface absorber," *Opt. Exp.,* vol. 25, no. 1, pp. 191–201, 2017.

[26] A. I. Kuznetsov, A. E. Miroshnichenko, M. L. Brongersma, Y. S. Kivshar, and B. Luk'yanchuk, "Optically resonant dielectric nanostructures," *Science,* vol. 354, no. 6314, 2016, Art. no. aag2472.

[27] C. Fang, Q. Yang, Q. Yuan, X. Gan, and Y. Hao, "High-Q resonances governed by the quasi-bound states in the continuum in all-dielectric metasurfaces," *Opto-Electron. Adv.,* vol. 4, no. 6, 2021, Art. no. 200030.

[28] A. Ahmadivand, B. Gerislioglu, R. Ahuja, and Y. K. Mishra, "Terahertz plasmonics: The rise of toroidal metadevices towards immunobiosensings," *Mater. Today*, vol. 32, pp. 108–130, 2020.

[29] Z. Li, Y. Xiang, S. Xu, and X. Dai, "Ultrasensitive terahertz sensing in all-dielectric asymmetric metasurfaces based on quasi-BIC," *J. Opt. Soc. Amer. B,* vol. 39, no. 1, pp. 286–291, 2022.

[30] W. Cen, T. Lang, J. Wang, and M. Xiao, "High-Q Fano terahertz resonance based on bound states in the continuum in all-dielectric metasurface," *Appl. Surf. Sci.,* vol. 575, 2022, Art. no. 151723.

[31] X. Jiang, W. Fan, X. Chen, and H. Yan, "Ultrahigh-Q terahertz sensor based on simple all-dielectric metasurface with toroidal dipole resonance," *Appl. Phys. Exp.*, vol. 14, no. 10, 2021, Art. no. 102008.

[32] Y. Yang et al., "Transient GaAs plasmonic metasurfaces at terahertz frequencies," *ACS Photon.*, vol. 4, no. 1, pp. 15–21, 2017.

[33] Y. Moritake, Y. Kanamori, and K. Hane, "Experimental demonstration of sharp Fano resonance in optical metamaterials composed of asymmetric double bars," *Opt. Lett.,* vol. 39, no. 13, pp. 4057–4060, 2014.

[34] J. Cui, X. Ma, M. Pu, Y. Guo, and X. Luo, "Extraordinary strong optical rotation in weak chiral metasurface," *Opto-Electron. Eng.,* vol. 47, no. 7, 2020, Art. no. 190052.